# Microstructural characterisation and high-temperature oxidation of laser powder bed fusion processed Inconel 625

Lewis, E.R.; Taylor, Mary; Attard, B.; Cruchley, N.; Morrison, A.P.C.; Attallah, M.M.; Cruchley, S.

*DOI:*
10.1016/j.matlet.2021.131582



*Document Version*
Peer reviewed version

*Citation for published version (Harvard):*
Lewis, ER, Taylor, M, Attard, B, Cruchley, N, Morrison, APC, Attallah, MM & Cruchley, S 2022, 'Microstructural characterisation and high-temperature oxidation of laser powder bed fusion processed Inconel 625', *Materials Letters*, vol. 311, 131582. https://doi.org/10.1016/j.matlet.2021.131582

***Microstructural Characterisation and High-Temperature Oxidation of Laser Powder Bed Fusion Processed Inconel 625***

*E. R. Lewis[a], M. P. Taylor[a], B. Attard[ab], N. Cruchley[c], A. P. C. Morrison[c*d], M. M. Attallah[a] and S. Cruchley[a]*

*Corresponding author: Dr S Cruchley*

*Email address: S.Cruchley@bham.ac.uk*

*[a]School of Metallurgy and Materials, University of Birmingham, B15 2TT, Birmingham, UK*

*[b]Department of Metallurgy and Materials Engineering, University of Malta, MSD 2080, Malta*

*[c]Manufacturing Technology Centre, Ansty Park, CV7 9JU, Coventry, UK*

*[d]Qdot Technology, Rutherford Appleton Laboratory, OX11 0QX, Didcot, UK*

**Formerly*

***Abstract***

Oxidation of Laser Powder Bed Fused (L-PBF) IN625 was studied in the as-built and heat-treated conditions. Following heat treatment, recrystallisation was observed with a large fraction of twin grain boundaries, and Nb-rich carbides decorated grain boundaries. Samples of L-PBF IN625 were exposed at 950°C in laboratory air and pressure for up to 504 h. An external chromia scale was formed, alongside a near-continuous δ-phase layer at the scale/alloy boundary. The kinetics of oxidation were similar to wrought IN625, but more closely followed cubic behaviour. It is suggested that the cubic behaviour was caused by the formation of the δ-phase layer.

***Keywords: Oxidation, Additive Manufacturing, Microstructure***

***1. Introduction***

Inconel 625 (IN625) is a chromia forming Ni-based superalloy with excellent corrosion resistance at temperatures up to 980°C [1]. A significant downside to its use, however, is poor machineability due to strain hardening, making the fabrication of complex geometries difficult [2]. Additive manufacturing is able to produce complex near-netshape components and IN625 lends itself well to Laser Powder Bed Fusion (L-PBF) due to its superior weldability over alloys such as CM247 [2,3]. Fast solidification rates,

common to L-PBF of the order of $10^6$ K/s, can produce fine dendritic microstructures with high dislocation densities giving rise to high tensile strength; often exceeding those of wrought IN625 [3,4]. Despite this, low nucleation barriers associated with high dislocation densities can lead to the accelerated formation of the brittle $Ni_3Nb$ δ-phase, following the segregation of Nb and Mo to interdendritic spaces [2,5]. Heat treatments are thus necessary to relieve the significant residual stresses and microsegregation formed during solidification.

The oxidation performance of as-built and solution heat-treated L-PBF IN625 oxidised at 900°C for 8-96 hours has been reported [6]. Each condition formed an adherent chromia scale embedded with clusters of Nb-rich oxide ($Nb_2O_5$). Significant microstructural evolution of the bulk of the alloy was shown, with large amounts of inter-/intragranular δ-phase forming. However, there is little research into the high temperature oxidation properties of L-PBF IN625 at longer exposures. This is an area where further research is required, as the use of additively manufactured components expands to more demanding applications. In this paper an investigation into the oxidation performance of L-PBF IN625 exposed at 950°C for up to 504 h, in the as-built and two heat treated conditions, is presented.

***2. Material and Methods***

Fully dense rods of L-PBF IN625 were built with an EOS M280 (400 W), using the default IN625_Performance_110 parameter set, with a layer height of 40 µm. Standard IN625 composition powders of sizes 15-45 µm were used. This was confirmed using a combination of LECO, ICP-MS (Inductively Coupled Plasma Mass Spectroscopy) and XRF (X-ray Fluorescence). The following heat treatments were applied [7]:

- Heat Treatment 1 (HT1): Anneal at 1038°C, 1h.
- Heat Treatment 2 (HT2): Solution treatment at 1177°C, 1 h.

Discs of the as-built and heat-treated conditions were cut to size (14 mm diameter, 2 mm height) using electrical discharge machining. Sample surfaces were ground, and polished to a 0.25 µm finish, and the

edges were chamfered. Samples were weighed using a five-figure calibrated balance and the dimensions of each sample were measured.

Prior to oxidation, samples were degreased in acetone, placed into open alumina crucibles, and inserted into pre-heated furnaces. Oxidation testing was carried out at 950°C in laboratory air and pressure for exposures of 24-504 h. At each interval, all samples were weighed, and selected samples were removed from each batch for inspection of the oxide film. The remaining samples were returned to the furnace. For cross-sectional analysis, samples were sputtered with gold, Ni-plated, and cold mounted in low shrinkage resin. These samples were then cut in half, ground and polished to a 0.25 µm finish.

Scanning Electron Microscopy (SEM) with Backscattered Electrons (BSE) was performed to examine the as-received microstructure and oxide films. Compositional information was gathered using Energy Dispersive X-ray Spectroscopy (EDS). Electron Backscatter Diffraction (EBSD) was conducted using step sizes and scanning areas of 2.5 µm and 680 µm by 400 µm for as-built samples, and 1.5 µm and 500 µm by 400 µm for heat-treated samples to obtain Inverse Pole Figures (IPFs) and average sample grain sizes. The percentages of Twin Grain Boundaries (TGBs) ($\theta$= 60°) were also measured. X-Ray Diffraction (XRD) was conducted using an automated X-Ray Diffractometer with a Cu kα radiation source, indexed between a 2$\theta$ range of 20-100°.

***3. Results and Discussion***

Figure 1 shows the as-received microstructures of the as-built and heat-treated L-PBF IN625. The as-built material demonstrated a fine cellular microstructure, with grains <30 µm in size. Fine columnar dendrites were found to extend parallel to the build direction.

The heat-treated microstructures were near-identical to wrought IN625, showing recrystallisation and equiaxed grains, <25 µm [8]. Globular precipitates decorated the grain boundaries in both conditions, enriched in Nb (7 wt.%) and Mo (17 wt.%). It has been shown in the literature that these precipitates are

NbC and MoC [5, 8]. HT2 showed a decrease in the number and size of precipitates compared to HT1, suggesting the successful redistribution of solute at the higher temperature.

The IPFs collected, Figure 1, showed that the heat-treatments resulted in an increased fraction of TGBs ($\theta$ = 60°), where HT2 yielded the largest fraction. An increased proportion of TGBs have been attributed to a significant improvement in the corrosion rate in IN600 by promoting the early formation of a chromia scale [9].

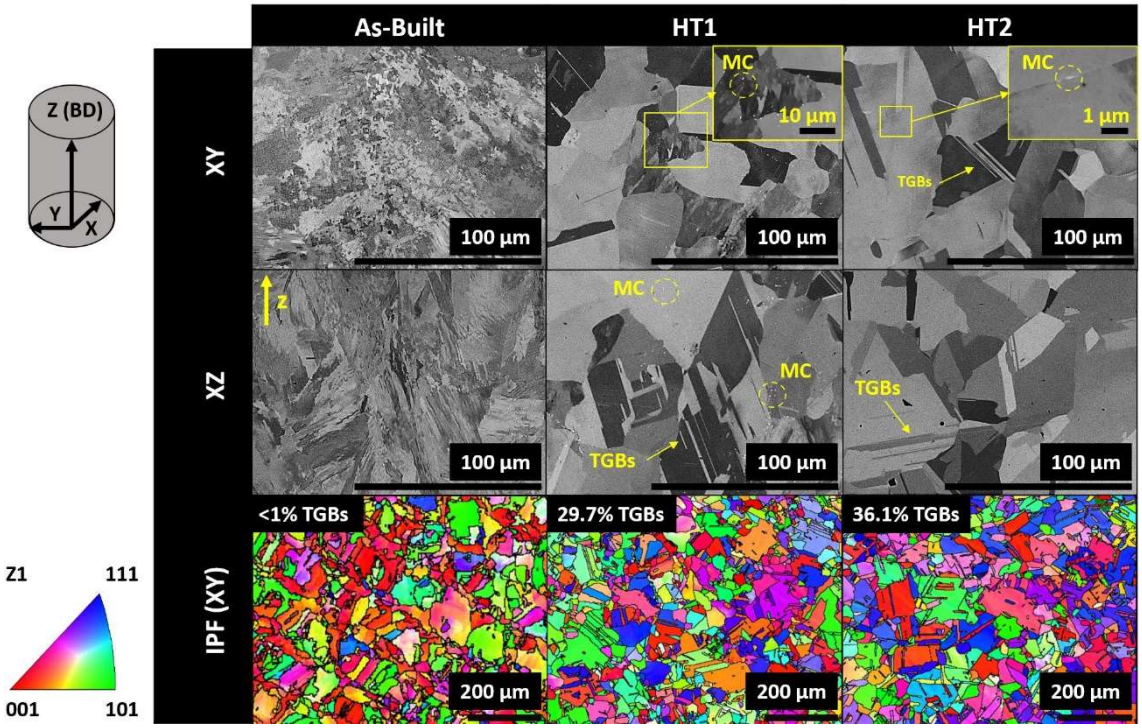


**Figure 1. SEM micrographs and IPFs of the as-received microstructure of as-built, HT1 and HT2 L-PBF IN625, where Z is indicated as the building direction. Highlighted are MC primary carbides and TGBs**.

The oxidation data collected for the as-built, HT1 and HT2 L-PBF IN625 was fit to the classical Wagner equation.

$$(\Delta m)^n = K'_n \cdot t \quad \textbf{(1)}$$

where Δm is specific mass gain/area (g.cm$^{-2}$), K'$n$ is the growth rate constant ((g.cm$^{-2}$)$^n$.s$^{-1}$), $n$ is the exponent, and t is the exposure time (s).

A value of $n$≈3 was found for all variants in this study, Table 1. The data was fit to Eq. 1 using

*n*=3 assuming cubic kinetics, and *n*=2 for a comparison to traditional parabolic behaviour, giving $K_C$ and $K_P$, respectively, Table 1. The mean mass change data with the cubic fit is shown in Figure 2, where it can be seen that the heat-treated variants showed slightly lower oxidation rates compared to the as-built alloy. Fitting the data to parabolic kinetics constants, Table 1, showed that all conditions oxidised at a comparable rate to wrought IN625, also included in Figure 1 [10], demonstrating the manufacturing route does not affect the oxidation properties. No noticeable spallation was observed in this study.

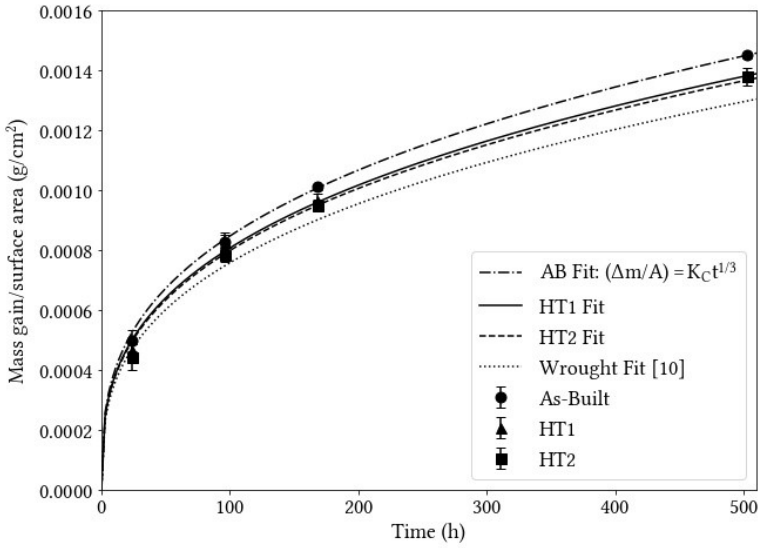


**Figure 2. Mean mass gain/area vs time for each condition of L-PBF IN625, oxidised at 950°C for up to 504 h, compared to wrought IN625 [10]. The lines show the fit to the cubic oxidation kinetics.**

**Table 1. Exponent *n*, parabolic, $K_P$, and cubic, $K_C$, rate constants for the oxide growth at 950°C.**

| Alloy Condition | $K_p$ ($g^2cm^{-4}s^{-1}$) | *n* | $K_c$ ($g^3cm^{-6}s^{-1}$) |
|---|---|---|---|
| **As-Built** | $1.25\times10^{-12}$ | 2.97 | $1.69\times10^{-15}$ |
| **HT1** | $1.14\times10^{-12}$ | 2.91 | $1.46\times10^{-15}$ |
| **HT2** | $1.12\times10^{-12}$ | 2.81 | $1.41\times10^{-15}$ |
| **Wrought IN625 [10]** | $1.17\times10^{-12}$ | 2.58 | $1.21\times10^{-15}$ |

BSE with EDS of cross-sections through the samples for all conditions examined, and the XRD patterns produced for the samples exposed for 504 h, Figure 3, showed that a porous and fairly uniform chromia scale was formed in all conditions. Beneath the chromia scale, a near-continuous Nb-rich layer formed at the scale/alloy interface, revealed to be δ-phase ($Ni_3Nb$). This phase is known to form on this alloy under oxidising conditions [10]. A slight enrichment of Mn was also noted within the scale across all

specimens and XRD identified small quantities of $MnCr_2O_4$ spinel forming on the heat-treated samples [8,11].

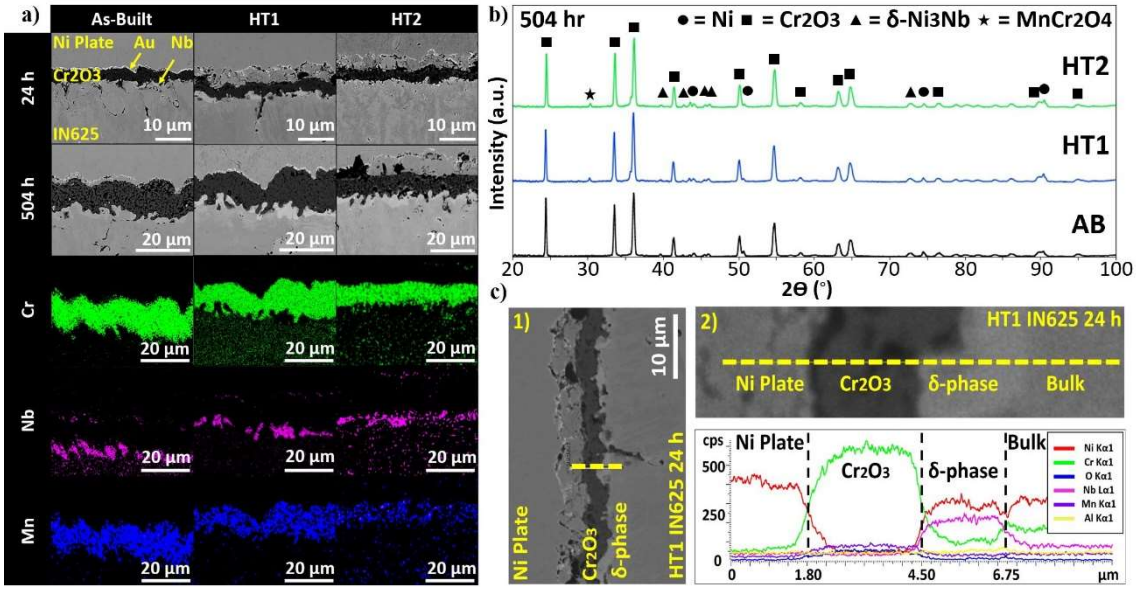


**Figure 3. a) BSE and EDS maps of cross-sections through as-built, HT1 and HT2 for 24 h and 504 h exposure at 950°C. b) XRD patterns of the as-built, HT1 and HT2 oxidised at 950°C at 504 h. c) BSE EDS line scan of the oxide scale and alloy sub-surface region formed for HT1, exposed for 24 h.**

Figure 3c shows the distribution of selected elements across the scale, δ-phase and into the bulk alloy for HT1, exposed for 24 h, confirming the low solubility of Cr in the δ-phase. The solubility of Cr in the δ-phase is ~4 wt.% at 950°C, also shown using Atom Probe Tomography [11]. Figure 3c also shows a slight enhancement of Cr in the bulk alloy adjacent to the δ-phase associated with the effect of the formation of the δ-phase. The presence of a continuous low Cr containing phase at the scale/alloy interface could reduce the supply of Cr from the alloy to the growing chromia layer. This reduction could have the effect of producing cubic-like oxidation kinetics. Further work is needed to assess the diffusion of Cr through the δ-phase including at the grain boundaries and is an aspect of further study.

### *4. Conclusions*

The following conclusions can be drawn:

- Heat-treated L-PBF IN625 showed a similar microstructure to wrought IN625 with large fractions of TGBs present.

- A surface chromia scale and a near-continuous underlying δ-phase layer formed at the outer surface of all alloy variants, as expected for this alloy.
- Parabolic rate constants determined for L-PBF IN625 showed a similar performance to the wrought alloy.
- Detailed analysis of the oxidation data demonstrated cubic mass change oxidation kinetic. It is suggested that the formation of the δ-phase layer is affecting these kinetics.

***Acknowledgements***

This work was supported by Parker Aerospace (UK).

***Funding***

This research did not receive any specific grant from funding agencies in the public, commercial, or not-for-profit sectors.

***References***

[1] A. S. Khanna, Handbook of Environmental Degradation of Materials, Elsevier, 2018, 117–132.

[2] F. Zhang, L. E. Levine, A. J. Allen, M. R. Stoudt, G. Lindwall, E. A. Lass, M. E. Williams, Y. dell, C. E. Campbell, Acta Mater. 152 (2018), 200–214.

[3] E. A. Lass, M. R. Stoudt, M. E. Williams, M. B. Katz, L. E. Levine, T. Q. Phan, T. H. Gnaeupel-Herold, D. S. Ng, Metall. Mater. Trans. A 48 (2017)5547–5558.

[4] A. Kreitcberg, V. Brailovski, S. Turenne, Mater. Sci. Eng., A, 689 (2017), 1–10.

[5] G. Lindwall, C. E. Campbell, E. A. Lass, F. Zhang, M. R. Stoudt, A. J. Allen, L. E. Levine, Metall. Mater. Trans. A, 50 (2019), 457–467.

[6] S. Parizia, G. Marchese, M. Rashidi, M. Lorusso, E. Hryha, D. Manfredi, S. Biamino, J. Alloys Compd. 846 (2020), 156418.

[7] AMS 2774 4G Heat Treatment Nickel Alloy and Cobalt Alloy Parts, 2020.

[8] K. Arnold, G. Tatlock, C. Kenel, A. Colella, P. Matteazzi, Mater. High Temp. 35 (2018), 141–150.

[9] P. Lin, G. Palumbo, U. Erb, K. Aust, Scripta Mater. 33 (1995), 1387–1392.

[10] A. Chyrkin, P. Huczkowski, V. Shemet, L. Singheiser, W. J. Quadakkers, Oxid. Met. 75 (2011), 143-166

[11] S. Pedrazzini, D. Child, G. West, S. Doak, M. Hardy, M. Moody, P. Bagot, Scripta Mater. 113 (2016), 51–54.